Molecular Therapy
Methods & Clinical Development
Original Article

Development of Intrathecal AAV9 Gene Therapy for Giant Axonal Neuropathy

Rachel M. Bailey,[1] Diane Armao,[2,3] Sahana Nagabhushan Kalburgi,[1,5] and Steven J. Gray[1,4,6]

[1]Gene Therapy Center, University of North Carolina at Chapel Hill, Chapel Hill, NC 27599, USA; [2]Department of Pathology and Laboratory Medicine, University of North Carolina at Chapel Hill, Chapel Hill, NC 27599, USA; [3]Department of Radiology, University of North Carolina at Chapel Hill, Chapel Hill, NC 27599, USA; [4]Department of Ophthalmology, University of North Carolina at Chapel Hill, Chapel Hill, NC 27599, USA

An NIH-sponsored phase I clinical trial is underway to test a potential treatment for giant axonal neuropathy (GAN) using viral-mediated *GAN* gene replacement (https://clinicaltrials.gov/ct2/show/NCT02362438). This trial marks the first instance of intrathecal (IT) adeno-associated viral (AAV) gene transfer in humans. GAN is a rare pediatric neurodegenerative disorder caused by autosomal recessive loss-of-function mutations in the *GAN* gene, which encodes the gigaxonin protein. Gigaxonin is involved in the regulation, turnover, and degradation of intermediate filaments (IFs). The pathologic signature of GAN is giant axonal swellings filled with disorganized accumulations of IFs. Herein, we describe the development and characterization of the AAV vector carrying a normal copy of the human *GAN* transgene (AAV9/JeT-GAN) currently employed in the clinical trial. Treatment with AAV/JeT-GAN restored the normal configuration of IFs in patient fibroblasts within days in cell culture and by 4 weeks in GAN KO mice. IT delivery of AAV9/JeT-GAN in aged GAN KO mice preserved sciatic nerve ultrastructure, reduced neuronal IF accumulations and attenuated rotarod dysfunction. This strategy conferred sustained wild-type gigaxonin expression across the PNS and CNS for at least 1 year in mice. These results support the clinical evaluation of AAV9/JeT-GAN for potential therapeutic outcomes and treatment for GAN patients.

INTRODUCTION

Giant axonal neuropathy (GAN) is a rare neurodegenerative disorder that typically presents in early childhood, with patients ultimately succumbing to disease by the third decade of life. First described by Asbury et al.[1] and Berg et al.[2] children with GAN initially present with gait abnormalities, sensory loss, and clumsiness from muscle weakness and ataxia, which progressively worsens, resulting in a complete loss of ambulation, compromised hand and arm function, dysarthria and dysphagia, and eventually death from respiratory failure.[3] Although classically described as a severe motor and sensory axonal neuropathy, CNS involvement is well described, with cases showing pathologic changes affecting the cerebellar cortex, brainstem, and posterior columns of the spinal cord.[4–6] GAN is caused by autosomal recessive, loss-of-function mutations in the *GAN* gene (reviewed by Johnson-Kerner[7]) that encodes the gigaxonin protein that plays a critical role in the organization and degradation of intermediate filaments (IFs).[8] A pathologic hallmark of GAN patients is massively enlarged axons filled with randomly arrayed, densely bundled IFs.[1,2,9] In GAN there is generalized dysfunction of many classes of IF proteins that are disorganized in multiple cell types including neurons, astrocytes, Schwann cells, perineurial cells, endothelial cells, muscle fibers, and fibroblasts.[4,10–12] The composition of inclusions is dependent on cell type and includes neurofilaments (NFs), peripherin, α-internexin, vimentin, glial fibrillary acidic protein (GFAP), nestin, desmin, and keratin.[2,8,13] For GAN patients, there is currently no approved therapy that targets the IF accumulations and neuronal dysfunction or halts the progression of disease.

Gene replacement therapy to express functional gigaxonin in cells has the potential to clear IF aggregates. Adeno-associated virus (AAV) has emerged as one of the safest and most commonly used vectors for gene replacement (reviewed by Kantor et al.[14]). Alternative routes of administration, coupled with specific targeting capabilities conferred by a variety of capsid choices, has positioned rAAV at the forefront of vectors used for gene delivery to neural tissue within the CNS (reviewed by Hocquemiller et al.[15]). AAV9 has emerged as one of the most frequently used serotypes for neurological disorders due to its ability to cross the blood-brain barrier and from its high transduction of neural tissue (reviewed by Murlidharan et al.[16]). We and others have shown that intrathecal (IT)-delivered AAV9 in large animals can transduce the majority of motor neurons in the spinal cord and the neurons of the dorsal root ganglia (DRG) with minimal targeting of virus to peripheral organs as compared to systemic delivery.[17–21] Our group was the first to show that viral-mediated *GAN* gene transfer restores the normal IF network in patient fibroblasts and in GAN knockout (KO) mice.[22] Additionally, IF aggregates can be reduced by expressing normal gigaxonin protein by plasmid transfection in patient fibroblasts[8] or by viral delivery in patient induced pluripotent stem cells (iPSCs)[23] and in cultured

Received 28 September 2017; accepted 9 February 2018;
https://doi.org/10.1016/j.omtm.2018.02.005.

[5]Present address: Brain Institute, Vanderbilt University, Nashville, TN 37232, USA

[6]Present address: Department of Pediatrics, University of Texas Southwestern Medical Center, Dallas, TX 75390, USA

Correspondence: Steven J. Gray, UT Southwestern Medical Center, NA2.508, 6000 Harry Hines Blvd., Dallas, TX 75390-8593, USA.
E-mail: steven.gray@utsouthwestern.edu

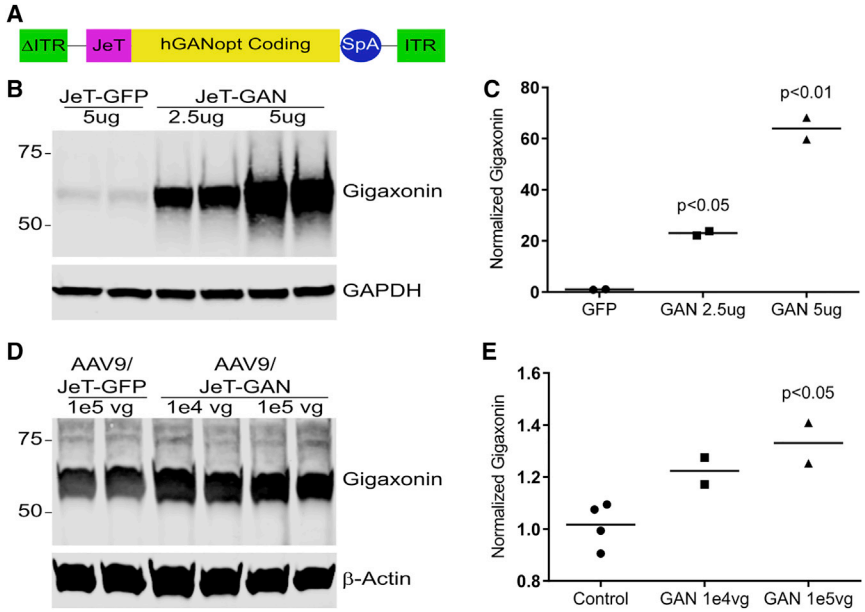

Figure 1. AAV9/JeT-GAN Construct Design for Expressing Human Gigaxonin

(A) Schematic diagram of the AAV/JeT-GAN gene transfer cassette using a JeT promoter, the full-length, codon-optimized human *GAN* cDNA, and the synthetic poly(A) tail (SpA). (B and C) Western blot and densitometry of gigaxonin expression from HEK293 cells transfected with the JeT-GAN plasmid or JeT-GFP control plasmid. (D and E) Western blot and densitometry of AAV9-permissive Lec2 cells treated with the indicated vectors at the indicated amounts per cell. (C and E) Values are mean ± SEM gigaxonin levels normalized to GAPDH or β-actin levels and relative to control (untransfected and GFP-treated) cells. Data were analyzed by one-way ANOVA with Bonerfonni's post-hoc analysis.

neurons from GAN KO mice.[24] Together, these studies provide support for *GAN* gene replacement therapy to treat GAN; however, these studies did not investigate approaches amenable for direct clinical translation and implementation.

We developed a vector designed for human therapy, which is a self-complementary (sc) AAV9 vector carrying a codon-optimized human *GAN* transgene whose expression is controlled by the minimal synthetic JeT promoter (AAV9/JeT-GAN). Here, we show that IT delivery of the AAV9/JeT-GAN vector in GAN KO mice has sustained levels of human gigaxonin expression for at least 1 year and that treated GAN KO mice have improved rotarod function and attenuated peripheral nerve pathology. Together, these preclinical data provide strong support for IT delivered, AAV9-mediated *GAN* gene transfer as a potential therapeutic approach for improved patient outcomes in GAN, a study which is currently being conducted as a phase I trial at the NIH Clinical Center (clinicaltrials.gov identifier: NCT02362438).

RESULTS

Design and Expression of a Gene Transfer Vector Expressing Gigaxonin

For downstream human application, we developed the AAV/JeT-GAN vector consisting of a minimal synthetic JeT promoter[25] driving the expression of codon-optimized human *GAN* cDNA that has a synthetic poly(A) tail[26] (Figure 1A). Given AAV packaging constraints,[27,28] use of the short JeT promoter allows sc packaging of the 1.9-kb gigaxonin coding sequence, which is predicted to stably transduce at least 10-fold more cells than single-stranded (ss) AAV.[29,30] The gene insert is bounded by the AAV2 inverted terminal repeats (ITRs), where one terminal repeat has the wild-type (WT) 144-nt sequence and the other ITR (ΔITR) is mutated to delete the AAV DNA resolution site and D sequence to direct preferential replication and packing of scAAV DNA sequences.[28] Since gigaxonin is normally expressed at very low levels,[12] the use of a minimal promoter is conceptually sound. HEK293 cells were transfected with our JeT-GAN plasmid to confirm expression of full-length gigaxonin protein (Figures 1B and 1C). Vector potency was assessed by infecting AAV9-permissive Lec2 cells with ∼1e4 or ∼1e5 AAV9/JeT-GAN vector genomes (vg) per cell for 48 hr. In AAV9/JeT-GAN-infected cells, gigaxonin protein was increased over the endogenous levels of vehicle or scAAV9/JeT-GFP-treated cells (1e4, ∼20%, and 1e5, ∼31%; $p < 0.05$) (Figures 1D and 1E). For proof-of-concept studies, we used an AAV/JeT-FLAG-GAN vector that has an N-terminal FLAG epitope tag inserted into the AAV/JeT-GAN vector (Figure S1A). Unfortunately, the addition of the FLAG epitope did not aid in the detection of gigaxonin protein (data not shown). We also used a high expression vector that we have previously described, which is the ss CMV-GAN construct that used a CMV enhancer/promoter, chimeric intron, myc-tagged gigaxonin coding sequence, and SV40 poly(A) tail (Figure S1B).[22] The uses of each vector are detailed in Table S1.

AAV-Packaged GAN Reduces IF Aggregates in Patient Fibroblasts

Cultured GAN patient fibroblasts have abnormal bundles and inclusions of vimentin IF protein (Figure 2A; Pena et al.[13]; Pena[31]). We and others have previously shown that use of a strong promoter to drive high expression of normal gigaxonin protein can restore the normal IF arrangement in GAN fibroblasts.[8,22] To test the efficacy of our JeT-driven vector, cells from three patients were infected with vehicle or $\sim 2.5 \times 10^5$ vg/cell of AAV2 vectors carrying either the JeT-GAN construct, a CMV-GAN construct, or a GFP reporter construct for 3 days. There was no difference in the percent of cells with inclusions between vehicle- and AAV2/GFP-treated cells, and results were combined to increase statistical power. Gigaxonin antibodies cannot be reliably used for immunocytochemistry or immunohistochemistry (IHC),[32] and epitope tagging did not aid the detection of gigaxonin

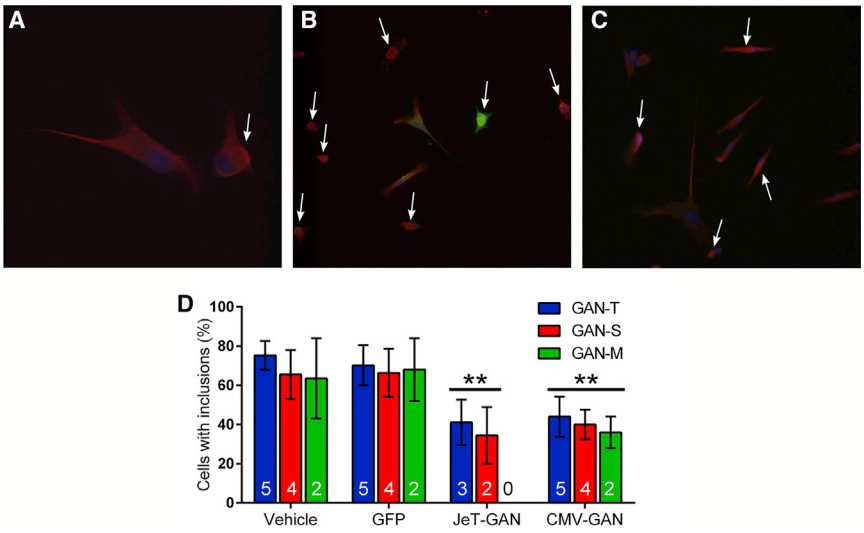

Figure 2. AAV/GAN Vectors Restore Normal IF Morphology in GAN Patient Fibroblasts

Cultures of fibroblasts from three patients (GAN-T, GAN-S, and GAN-M) were infected with either vehicle, AAV2/JeT-GFP, AAV2/JeT-FLAG-GAN, or AAV2/CMV-GAN for 72 hr. Cells were then stained for vimentin (red), GFP (green), and DAPI to visualize the nuclei (blue). (A–C) Representative images of GAN-S fibroblasts. Arrows indicate inclusions. (A) Enlarged view of normal (left) and GAN-specific (right) distribution of vimentin in vehicle-treated GAN fibroblasts to illustrate how inclusion-negative and inclusion-positive cells were scored. (B) GFP staining of GFP-treated patient cells shows the relative transduction efficiency of AAV2 in both normal and inclusion-bearing cells. (C) GAN fibroblasts treated with AAV2/FLAG-JeT-GAN show a reduction in the number of cells containing vimentin inclusions. (D) Quantification of the percent of cells containing inclusions for each patient culture. Values are means ± SEM for each group. One-way ANOVA with Bonferonni's post-hoc analysis of each treatment condition compared to control cells (vehicle and GFP-treated) (**$p < 0.01$). The number of trials performed per condition are indicated at the base of each bar.

(data not shown), so the transduction efficiency was assessed using the GFP reporter construct. The transduction efficiency of AAV2/JeT-GFP in GAN fibroblasts was ~50%, and GFP was found in both cells with normal and abnormal vimentin arrangements (Figure 2B). Compared to control cells, treatment with both AAV2/JeT-GAN and AAV2/CMV-GAN restored a normal pattern of IF distribution and reduced the percentage of cells with vimentin inclusions (Figures 2C and 2D). In this system, use of the weak JeT promoter was equally beneficial as using the stronger CMV promoter (CMV data was previously published in Mussche et al.[22]). Given that the transduction efficiency was approximately 50%, these results suggest that nearly all of the cells infected by the viral vector were rescued within 3 days.

Direct Brain Injection of AAV9/GAN Decreases NF Aggregates

The results from the patient fibroblasts demonstrate the ability of the JeT-GAN construct to clear vimentin aggregates from mitotic cells *in vitro*. GAN KO mice are pathologically characterized by axons filled with disorganized NFs and IF aggregates throughout the CNS.[33,34] As an initial proof-of-concept that our JeT-GAN vector can clear another type of IF aggregate in post-mitotic cells *in vivo*, aged GAN KO mice received a unilateral brain injection into the border of the striatum and cortex with a mix of AAV9/JeT-FLAG-GAN (1.25×10^9 vg) and AAV9/JeT-GFP (1.25×10^9 vg) (mouse cohort 1; see Table 1 for summary of experimental cohorts, treatments, and assays). Co-injection of a GFP vector was included to mark the transduced area, since antibody reagents are not suitable to detect gigaxonin by IHC and the FLAG epitope did not aid in the detection of gigaxonin (data not shown). Four weeks post-injection, GFP staining showed that viral transduction was highest near the site of injection and was largely restricted to the injected hemisphere (Figure 3A). NF inclusions were significantly reduced in the GAN KO brain after treatment with AAV9/JeT-GAN ($F(2, 6) = 28.17$, $p < 0.001$), particularly in the striatum ($p < 0.001$) and cortex ($p < 0.05$), while there was no change in the number of inclusions in the control area (Figures 3B to 3E). While direct intraparenchymal injection of the vector is not proposed as a translatable therapeutic approach, the high transduction efficiency of this route afforded a relevant histopathologic effect that was unambiguously visualized and scored. We conclude that AAV9/JeT-GAN is capable of clearing longstanding IF aggregates from post-mitotic cells.

IT Delivery of AAV9/JeT-GAN Attenuates Rotarod Dysfunction

To improve the quality of life and survival of GAN patients, the primary targets for gene replacement therapy are thought to be the brainstem and the motor-sensory neurons of the spinal cord and DRG. Direct injections are invasive surgical procedures with minimal spread of virus from the sites of injection that would be difficult to translate to clinical application for a disease thought to require widespread CNS and peripheral nervous system (PNS) correction. We therefore evaluated the safety and benefit of IT delivery of AAV9/JeT-GAN in aged GAN KO mice, after the onset of GAN-specific pathology, as a clinically relevant treatment approach. GAN/Y KO mice (deletion of *GAN* exons 3–5) were used as our primary animal model, as they were initially reported to have a severe phenotype that included the onset of a motor phenotype around 9 months of age,[33] although others have reported that the phenotype of the GAN/Y KO model is much less robust.[35] Experiments were also conducted in the GAN/J mouse (deletion of *GAN* exon 1), although no behavioral phenotypes were described in this model.[34] Mice were injected with a dose 5×10^{10} vg of AAV9/JeT-GAN delivered via a single IT injection around 12 months of age (GAN/Y; cohort 2) (Figure 4A) or between 14 and 16 months of age (GAN/J; cohort 3) (Figure 4B), and rotarod performance was tested monthly. No adverse effects on overall health or weight were apparent in control or IT-treated GAN KO mice (data not shown). In our colony, aged

Table 1. GAN KO Mouse Cohorts, Treatments, and Assays Discussed in the Text

Cohort	Model	Experimental Group	n	Dose of Injection (vg)	Age of Injection (months)	Analyses
1	GAN/Y KO	unilateral brain AAV9/JeT-GFP + AAV9/JeT-FLAG-GAN	3	1.25×10^9 vg + 1.25×10^9 vg	20	NF quantification in brain
2	GAN/Y Het	no vector	10	–	–	rotarod, DRG IF inclusions, gigaxonin expression
		vehicle	8	–	12 or 18	
	GAN/Y KO	vehicle	9	–	12 or 18	
		AAV9/JeT-GAN	8	5×10^{10}	12	
3	GAN/J Het	vehicle	10	–	14–16	rotarod, gigaxonin expression
		AAV9/JeT-GAN	9	5×10^{10}	14–16	
	GAN/J KO	vehicle	10	–	14–16	
		AAV9/JeT-GAN	11	5×10^{10}	14–16	
4	GAN/Y Het	no vector	3	–	–	sciatic nerve morphology
	GAN/Y KO	no vector	1	–	–	
		AAV9/JeT-GFP	5	1.2×10^{10}	18	
		AAV9/JeT-FLAG-GAN	6	1.2×10^{10}	18	

GAN/Y KO mice had late-onset accelerating rotarod deficits as compared to normal control mice (main effect of genotype, $F(1, 83) = 30.58$, $p < 0.0001$), with a significant deficit in performance at 20 months of age (post-hoc analysis following two-way ANOVA, $p < 0.05$) (Figure 4C). Treatment with AAV9/JeT-GAN in GAN/Y KO mice did not completely rescue rotarod performance as compared to normal control mice (main effect of treatment, $F(1, 96) = 15.01$, $p < 0.001$); however, treatment delayed the onset of rotarod dysfunction until 22 months of age (post-hoc analysis of each month following two-way ANOVA, $p < 0.01$) (Figure 4D). Additionally, there was a small but significant improvement in the overall rotarod performance of GAN/Y KO mice with IT treatment of AAV9/JeT-GAN as compared to vehicle-treated mice (main effect of treatment, $F(1, 55) = 4.174$, $p < 0.05$) (Figure 4E). In agreement with the original description of this model,[34] GAN/J KO mice did not have a rotarod deficit up to 24 months of age, and treatment with AAV9/JeT-GAN did not adversely affect rotarod performance of control or KO mice as compared to vehicle-treated mice of the same genotype (Figure 4F). Together, these results support that IT injection of AAV9/JeT-GAN is well tolerated in mice and that it can attenuate rotarod dysfunction in GAN/Y KO mice.

IT Delivery of AAV9/JeT-GAN Results in Long-Term Gigaxonin Expression

A benefit of AAV-based gene replacement therapy is that AAV-delivered DNA persists indefinitely in the nucleus of post-mitotic cells,[36] so we analyzed gigaxonin expression in IT-injected mice up to 1 year post-injection. Commercially available gigaxonin antibodies are poor at detecting low gigaxonin protein levels and detect multiple non-specific bands by western blotting.[32] Accordingly, while we were able to detect gigaxonin protein in the lumbar cord of the majority of the AAV9/JeT-GAN-treated GAN KO mice that we analyzed (Figure S2), a more sensitive method (qPCR analysis of vector DNA and GAN_{opt} mRNA) was used to assess the overall biodistribution and expression of the vector. We found that the vector DNA (Figure S3) and codon-optimized gigaxonin mRNA (Figure 5) were concentrated closest to the site of injection in the spinal cord and DRG and were detected at much lower levels in multiple brain regions and to a small extent in the sciatic nerve of both GAN/Y (cohort 2) and GAN/J mice (cohort 3). The IT route concentrated vector expression in CNS tissues as compared to an intravascular route of administration,[30] but relatively high amounts of vg persisted in peripheral organs, particularly in the liver and to a lesser extent in the heart. We also found that AAV-treated normal control and GAN/J KO mice had similar vector biodistribution levels (Figure S3) and expression of the human gigaxonin transgene except for in the cervical spinal cord, where normal mice had significantly more transcripts ($p < 0.05$) (Figure 5B). Overall, IT delivery of AAV9/JeT-GAN results in persistent gigaxonin expression in the CNS and peripheral nerves of GAN KO and normal mice.

IT GAN Gene Therapy Reduces DRG Neuronal IF Inclusions

We next examined IF pathology in lumbar DRG, one of the primary targets for gene therapy in patients. H&E-stained sections of DRG from untreated aged GAN KO mice revealed numerous, brightly eosinophilic, IF inclusion-bearing neurons within the small dark neuron population of DRG that were absent in normal control mice DRG (Figures 6A and 6B). Examination of treated GAN KO mice (cohort 2) revealed a significant reduction of neuronal perikaryal IF inclusions in the DRG as compared to vehicle-injected mice (Figures 6B to 6D). This improved pathology in treated mice was 12 months post-injection, indicating an enduring benefit of IT delivery of AAV9/JeT-GAN.

Sciatic Nerve Ultrastructure Is Preserved by AAV9/JeT-GAN Gene Therapy

To further investigate the therapeutic benefit of IT-delivered AAV9/JeT-GAN, we examined the sciatic nerves from GAN mice injected at

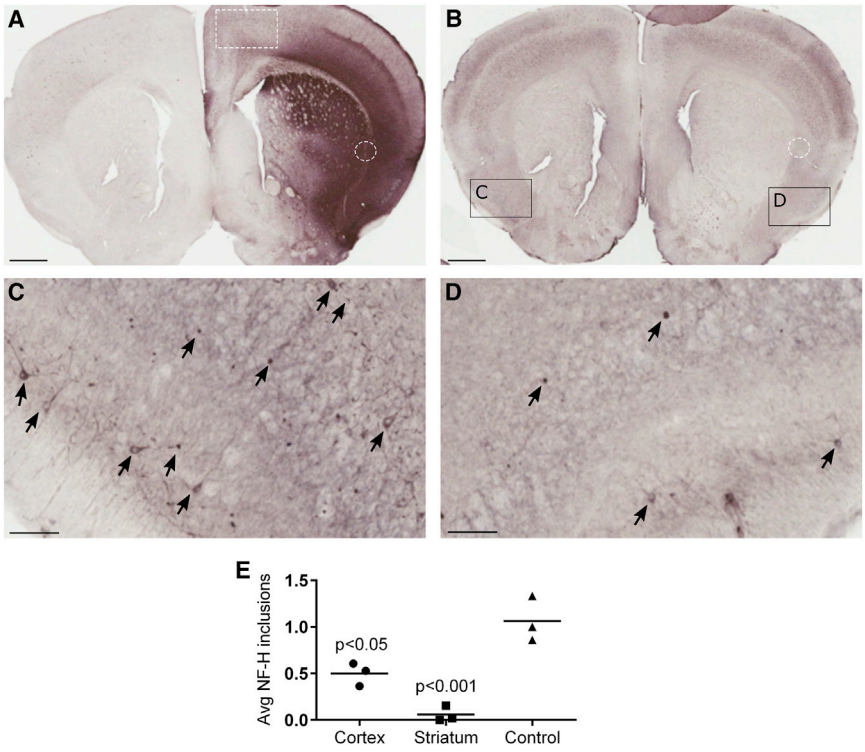

Figure 3. AAV9/JeT-GAN Reduces NF Inclusions in Cortical and Striatal Neurons

Twenty-month-old GAN/Y KO mice received a unilateral brain injection into the border of the striatum and cortex of a mix of AAV9/JeT-FLAG-GAN and AAV9/JeT-GFP and harvested 4 weeks post-injection (cohort 1). (A) A representative image of GFP staining shows that AAV9 vector spread decreased with distance from the injection site and was substantially reduced in the uninjected hemisphere. The white hashed box outlines the "control" area that was not efficiently transduced by AAV9, and the white dashed circle shows the injection site. (B) A representative image of NF staining shows that compared to the untreated hemisphere (C), NF inclusions are greatly reduced in the treated side (D). (E) Quantification of NF inclusions in the treated hemisphere, normalized to the number of inclusions in the corresponding area of the untreated hemisphere of each mouse. Data are means ± SEM for each group, n = 3 mice. One-way ANOVA with Bonferonni's post-hoc analysis. (A and B) Scale bars represent 1 mm. (C and D) Arrows point to examples of NF inclusions, and scale bars represent 0.1 mm.

18 months of age with either 1.2×10^{10} vg AAV9/JeT-GFP or 1.2×10^{10} vg AAV9/JeT-FLAG-GAN and harvested at 24 months of age (cohort 4). No differences in the sciatic nerve pathology of untreated and AAV9/JeT-GFP-treated GAN KO mice were observed. In agreement with previous studies, sciatic nerve sections showed focal and diffuse patterns of fiber loss with scattered enlarged axons surrounded by abnormally thin myelin sheaths in control GAN KO mice as compared to normal control mice (Figure S4).[33–35] Qualitative analysis of the *GAN*-treated mice revealed an overall increase in fibers compared to the control KO mice, with a notable preservation of large diameter myelinated fibers (Figure S4). Electron microscopic (EM) examination of sciatic nerves from normal control mice were unremarkable (Figure S5). Qualitatively, control GAN KO sciatic nerves revealed fiber loss preferentially involving small-diameter myelinated fibers and unmyelinated fibers (Figure 7A). Large-diameter myelinated fibers appeared relatively intact, although an overall increased density of NFs was present. There were many enlarged axons distended by disorganized bundles of NFs and surrounded by a disproportionately thin myelin sheath (Figure 7B), and scattered regenerating clusters were identified. A novel finding of our EM analyses were IF accumulations within perineurial cells of the nerve sheath, and abundant IF accumulations within Schwann cell cytoplasm associated with both unmyelinated and myelinated fibers (Figure 7C).

In *GAN*-treated KO mice, there was relative preservation of unmyelinated fibers and small-diameter myelinated fibers compared to control GAN KO mice, and the overall sciatic nerve ultrastructure of treated GAN KO mice was closer to that of normal mice (Figure 7D). While there was an overall decrease in the accumulation of NFs throughout *GAN*-treated nerve fibers as compared to control-treated KO fibers, an increased density of regularly aligned NFs within large-diameter myelinated fibers (Figure 7E) and unmyelinated fibers of mice as well as scattered foci of IF accumulation within Schwann cell cytoplasm were noted (Figure 7E). Treated KOs showed many profiles of normal appearing Schwann cells (Figure 7F). In several *GAN*-treated KO mice, abundant regenerating clusters were a prominent feature (Figure S6). Together, these findings indicate that there were signs of an axonal regenerative response to nerve fiber injury and that there was a partial rescue of normal axonal and Schwann cell ultrastructural anatomy in the mice treated at 18 months of age.

DISCUSSION

GAN is a rare, devastating neurological disorder that begins in early childhood at 3–4 years of age, generally manifesting with sensory ataxia. In the PNS the disease progressively affects sensory and motor nerves.[3–5] By the end of the second decade of life, patients typically are wheelchair dependent with limited use of the arms and little to no use of their legs, and during the second decade a tracheostomy or other means of ventilation, as well as a feeding tube, are often necessary. The CNS is also involved in GAN, as MRI may show white matter abnormalities in the brain and cerebellum and eventually severe atrophy of the brainstem and spinal cord in later stages of the disease. Death typically occurs by the third decade of life, as there is no treatment.[7] In response to the pressing needs of GAN children and their families, our group has worked closely with the NIH/NINDS clinical team (directed by Dr. Carsten Bönnemann) and Hannah's Hope Fund to translate our AAV-based *GAN* gene therapy from preclinical development to a phase 1 clinical trial that is currently being conducted

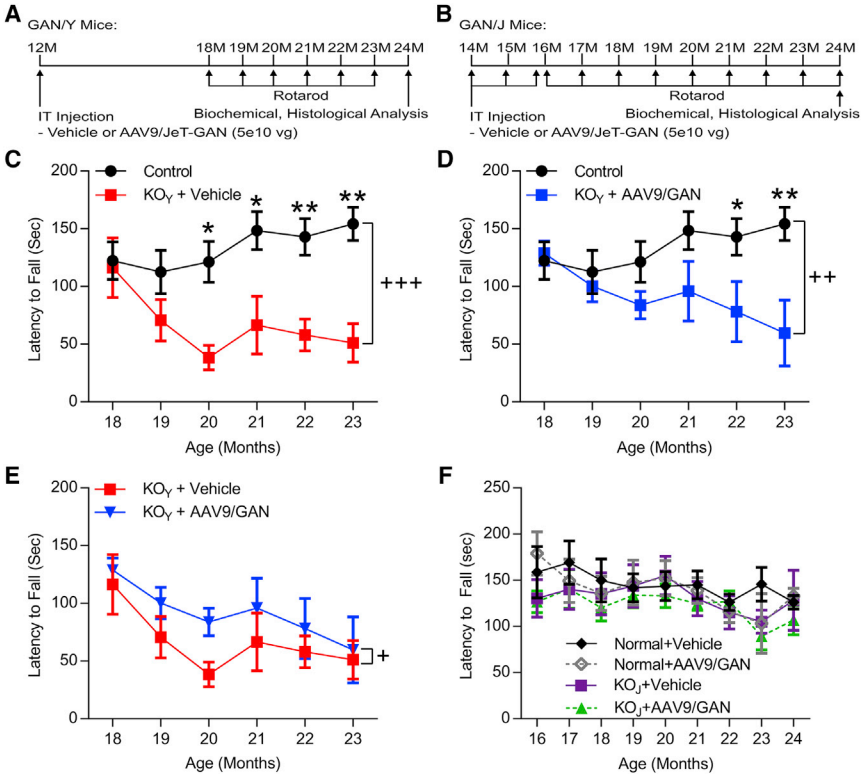

Figure 4. IT Delivery of AAV9/JeT-GAN in GAN KO Mice Attenuates Rotarod Deficits

(A) Study design for GAN/Y KO (cohort 2) and (B) for GAN/J KO mice (cohort 3). (C) Aged GAN/Y KO mice (red) have significantly impaired rotarod performance as compared to normal control littermates (black) beginning at 20 months of age. (D) Treatment with AAV9/JeT-GAN delays a significant rotor deficit in GAN/Y KO mice (blue) as compared to normal control mice (black) until 22 months of age. (E) Over the course of testing, treatment with AAV9/JeT-GAN (blue) significantly improves rotarod performance as compared to vehicle-treated GAN KO mice (red). (F) No difference in rotarod performance was found between aged normal control (black) and vehicle-treated GAN/J KO mice (purple). Treatment with AAV9/JeT-GAN did not affect the motor performance of either control (gray) or GAN KO mice (green). Data are means ± SEM for each group (GAN/Y, n = 18 normal controls, 8 KO + vehicle, and 7 KO + AAV9/GAN; GAN/J, n = 10 normal + vehicle, 9 normal + AAV9/GAN, 10 KO + vehicle, and 11 KO + AAV9/GAN). Two-way ANOVA (age × group); main effect of group, +$p < 0.05$, ++$p < 0.01$, +++$p < 0.001$; Bonferonni's post-hoc analysis of age: *$p < 0.05$, **$p < 0.01$.

at the NIH Clinical Center: Intrathecal Administration of sc AAV9/JeT-GAN for the Treatment of Giant Axonal Neuropathy (clinicaltrials.gov identifier: NCT02362438). Here, we describe the design of a translationally relevant gene therapy for GAN and present preclinical studies and efficacy outcomes supporting IT delivery of AAV9/JeT-GAN as a treatment for GAN.

An ideal safe and effective treatment for GAN requires a level of gigaxonin expression that is sufficient for resolving IF aggregates without abolishing the normal IF cytoarchitecture. Gigaxonin is found at extremely low levels in humans (~7,500 molecules/lymphoblast cell),[12] and loss of normal IF structure has been reported in cultured fibroblasts and neurons when a strong promoter was used to drive transgenic gigaxonin expression well-above physiological levels.[8,24] Our first-generation *GAN* gene replacement vector used the strong CMV promoter to drive expression,[22] so here we investigated the use of the weaker synthetic JeT promoter.[25] The JeT promoter allowed for the packaging of the *GAN* gene in a more efficient sc vector.[29,30] As expected, infection with AAV9/JeT-GAN in Lec2 cells and injection in mice resulted in low gigaxonin expression. When AAV2/JeT-GAN vectors were tested in patient fibroblasts, we found that the weak JeT promoter was equally efficient at clearing IF aggregates as the stronger CMV promoter and that normal IF cytoskeleton was not ablated. The IF phenotype was rescued in patient fibroblasts within 3 days of *GAN* infection, suggesting that gigaxonin is able to rapidly clear IF inclusions. Extending this fibroblast rescue to an *in vivo* proof of concept, direct brain injection of AAV9/JeT-GAN reduced NF inclusions in the brains of aged GAN KO mice within 4 weeks of injection and without any signs of toxicity. Overall, the AAV/JeT-GAN vector provided levels of gigaxonin sufficient for clearing IF aggregates without an appreciable loss of the normal cytoskeleton.

To improve the quality of life and survival of GAN patients, the primary targets for gene replacement therapy are thought to be the spinal cord, DRG, and brainstem. Our group and others have shown that IT-delivered AAV9 transduces most motor and sensory neurons in the spinal cord and DRG and some neurons within the brainstem. IT delivery has the added benefits of reduced targeting of virus to peripheral organs and avoidance of AAV9-neutralizing antibodies in the blood as compared to systemic delivery.[17–19,37] The biodistribution of AAV9 in small and large animals has been validated across multiple labs,[19,21,38] and here we show that the distribution of gigaxonin expression 1 year post-IT injection of AAV9/JeT-GAN in mice agrees with that data. Further, IT delivery of vector is a minimally invasive route of injection and is scalable to humans. In our study, mice were given a single IT injection of 5×10^{10} vg, which given a CSF volume of 0.035 mL, is a dose of 1.4×10^{12} vg/mL CSF. When extrapolated to larger animals by CSF volume, in non-human primates (NHPs) (12 mL CSF) this equates to a dose of $\sim 1.7 \times 10^{13}$ vg, and in humans (140 mL CSF) this equates to a dose of 1.96×10^{14} vg. Meyer et al.[21] used a comparable route of administration with our approach, and at a dose of 2×10^{13} in non-human primates they reported 55%–80% spinal cord motor neuron transduction along with widespread brain transduction. While IT treatment in GAN/Y KO mice improved rotarod function as compared to

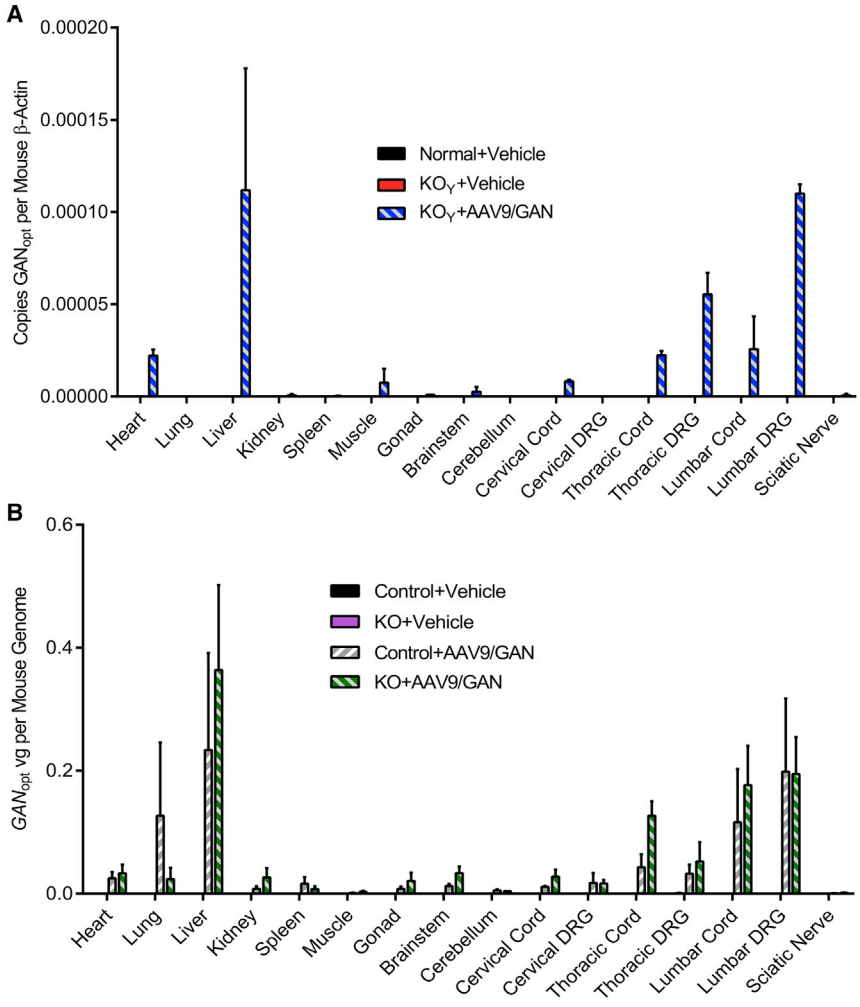

Figure 5. Gigaxonin Expression Persists in Aged Mice IT-Injected with AAV9/JeT-GAN

Gigaxonin gene expression was assessed by measuring the codon-optimized human gigaxonin mRNA in each tissue sample from GAN/Y mice injected at 12 months of age and harvested at 24 months of age (cohort 2) (A) and from GAN/J mice injected at 14–16-months of age and harvested at 24 months of age (cohort 3) (B). Mouse β-actin mRNA was measured as an internal control. β-actin was detected in all samples, and codon-optimized human gigaxonin mRNA was not detected in vehicle-injected animals. Data are means ± SEM for each group (GAN/Y: n = 2 per group; GAN/J: n = 3 per group). Multiple unpaired Student's t tests were performed on *GAN*-treated animals, *$p < 0.05$.

vehicle-treated KO mice, by 23 months of age, both groups had comparable performance. This incomplete rescue may have resulted from testing animals close to the end of their natural lifespan (24 months old) and/or from using a dose not sufficient to completely treat cells critical for rotarod function. Cross-correction between treated cells and their neighbors is not expected, as gigaxonin is not secreted, so the percentage of cells that are transduced by a single injection of AAV9/JeT-GAN needs to be increased. Studies of IT delivery of AAV9 in mice and NHPs show a dose response wherein a higher dose correlated to a higher percentage of transduced cells.[20,21,38] Notably, none of these studies reached a saturating dose of AAV9, and we have shown that our construct design for GAN is unlikely to introduce overexpression-related toxicity. Together, these data support the safety of increasing the dose administered in patients in order to increase the percent of transduced cells in the spinal cord and brain and maximize the therapeutic benefit.

As further proof of concept that IT delivery is a relevant approach to humans, IT delivery of AAV9/JeT-GAN decreased DRG neuronal perikaryal inclusions and IF aggregates in sciatic nerve axons and Schwann cells. Ultrastructural examination of GAN KO mouse peripheral nerve showed axonal loss preferentially involving small-diameter myelinated fibers and unmyelinated fibers with severe and pronounced IF accumulation within axons and Schwann cell cytoplasm. Treated GAN KO mice showed relatively well-preserved unmyelinated fibers and large-diameter myelinated fibers with overall increased profiles of normal-appearing Schwann cells when compared to GAN KOs. Of particular note in several mice within the treated GAN KO cohort was the prominence and abundance of new axonal sprouts, signified by regenerating clusters. When clinically evaluating peripheral nerve biopsies, the *absence* of regenerating clusters may indicate neuronal death,[39] and while regenerating clusters have been reported in human GAN, they are not a prominent feature.[40,41] Thus, in the context of the present research findings, *GAN* gene therapy provides a strategy for promoting new axonal sprouting and regeneration and degrading IF accumulations.

Here, we report the preclinical therapeutic development and validation studies supporting the initiation of an ongoing GAN phase 1 clinical trial that has pioneered the use of IT-delivered rAAV vectors for gene replacement therapies for childhood CNS disorders. We show that treatment with the novel AAV/JeT-GAN vector restored the normal arrangement of IF in patient fibroblasts within days in cell culture and by 4 weeks in the brains of GAN KO mice. IT treatment of aged GAN KO mice preserved sciatic nerve ultrastructure, decreased IF inclusions, and attenuated rotarod dysfunction. This strategy conferred sustained gigaxonin expression across the CNS and PNS for at least 1 year. We report the absence of any decreased rotarod performance in GAN/J mice and the absence of additional pathology in treated GAN mice within this study, supporting the overall safety of the approach. Additional supporting investigational

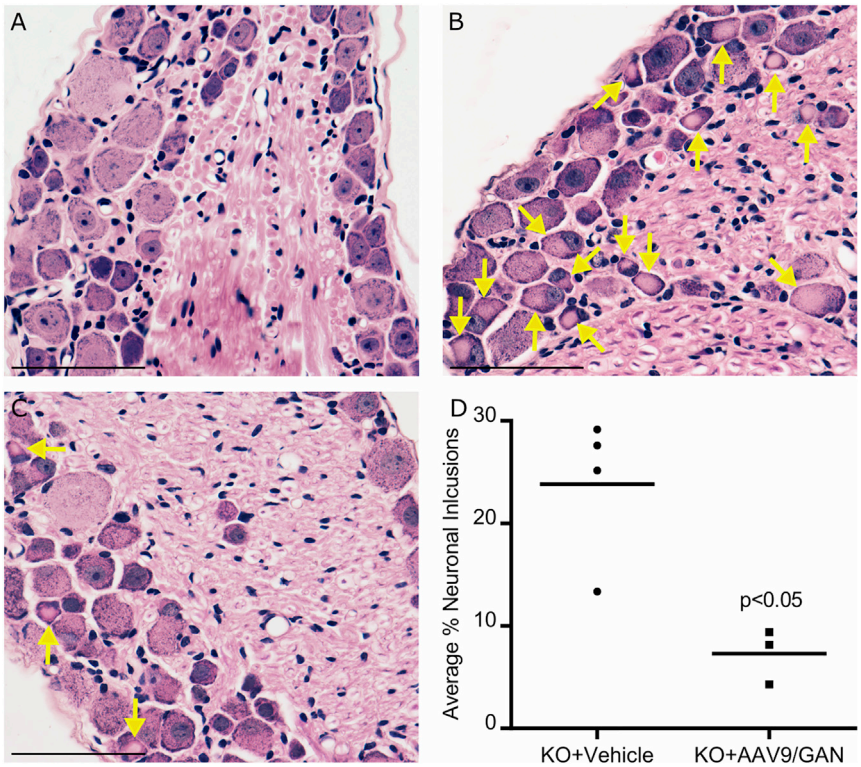

Figure 6. AAV9/JeT-GAN Reduces IF Inclusions in the DRG of GAN/Y KO Mice

Representative images of light microscopic evaluation of lumbar DRG in 24-month-old normal control (A), vehicle IT-injected GAN /Y KO mice (B), and AAV9/JeT-GAN IT-injected GAN/Y KO mice (C). H&E staining shows unremarkable DRG neurons in control mice (A) versus abundant, brightly eosinophilic inclusion-bearing neurons of vehicle-treated GAN/Y KO mice (B). Neuronal inclusions in *GAN*-treated mice were significantly reduced compared to vehicle-treated GAN KO mice (C and D). Scale bar represents 61 μm. Arrows indicate neuronal inclusions. Data was analyzed by unpaired Student's t test.

new drug (IND)-enabling toxicology studies for the phase I trial are not reported herein. In summary, preclinical evidence supports the potential benefit of IT AAV9/JeT-GAN gene therapy for GAN, a devastating pediatric disease that heretofore was without treatment options.

MATERIALS AND METHODS

Plasmids

Three plasmids were used for gigaxonin expression: (1) CMV-GAN, (2) JeT-FLAG-GANopt, and (3) JeT-GANopt. The CMV-GAN construct is as described.[22] The JeT-FLAG-GAN used a minimal synthetic JeT promoter,[25] an N-terminal FLAG tag, a human codon-optimized gigaxonin sequence (DNA2.0 Menlo Park, CA), and a short synthetic poly(A) tail.[26] The FLAG tag did not aid in the detection of gigaxonin and was removed to create an untagged JeT-GAN construct. A sc JeT-GFP vector packaged EGFP under control of the JeT promoter.

Virus Production

AAV vectors were produced using methods developed by the University of North Carolina (UNC) Vector Core facility, as described.[42] The purified AAV was dialyzed in PBS supplemented with 5% D-Sorbitol and an additional 212 mM NaCl (350 mM NaCl total). Vector was titered by qPCR[43] and confirmed by PAGE and silver stain. The recombinant vectors in these studies were sc vectors, except for the ss AAV/CMV-GAN vector. The vectors were packaged in AAV2 for fibroblast studies and in AAV9 for Lec2 and animal studies.

Cell Cultures

GAN patient fibroblast cell line "H" had a homozygous deletion (c.1647-8680_*258del), "M" had heterozygous mutations (p.S52G and C393X) and "T" had a homozygous missense mutation (p. Ala49Glu). Patients were clinically verified and had typical GAN symptoms. Lec2 cells and GAN fibroblasts were maintained in minimum essential medium (MEM)-alpha with and without nucleosides, respectively (Gibco, 12561 and 12571) and HEK293 cells were maintained in DMEM (Gibco, 11995). Media was supplemented with 10% fetal bovine serum and penicillin-streptomycin, and cells were maintained at 5% CO_2 and 37°C.

Vector Expression Studies in Cells

For JeT-GAN plasmid expression studies, HEK293 cells were plated and transfected with 2.5 or 5 μg of each plasmid using Lipofectamine 2000 (Invitrogen). For AAV9/JeT-GAN expression studies, Lec2 cells were infected with 1e4 or 1e5 vg/cell for 48 hr. Cells were collected, sonicated in lysis buffer (50 mM Tris-HCl, [pH 7.5], 150 mM NaCl, 100 μM DTT, 1 mM PMSF, 1% protease inhibitors cocktail [Thermo Scientific], and 1% phosphatase inhibitor cocktails 2 and 3 [Sigma]) and centrifuged at 16,000 × *g* for 15 min. Protein concentration was determined using a bicinchoninic acid (BCA) protein assay (Pierce). Either 30 μg (plasmid expression) or 80 μg (viral expression) of protein was loaded onto 10% gels (Bio-Rad), separated by SDS-PAGE and transferred to nitrocellulose membranes. Blots were probed with gigaxonin antibody (1:300; Sigma, SAB4200104) and either glyceraldehyde 3-phosphate dehydrogenase (GAPDH) antibody (1:10,000; Meridian Life Science) or β-actin antibody (1:10,000; Abcam, ab6276) overnight at 4°C and then with donkey anti-rabbit (1:5,000; LI-COR Biosciences, IRDye 800CW) and donkey anti-mouse (1:10,000; LI-COR Biosciences, IRDye 680CW). Immunofluorescence was imaged using a LI-COR infrared scanner and densitometry analyzed using Image Studio Lite (v. 5.2.5; LI-COR Biosciences).

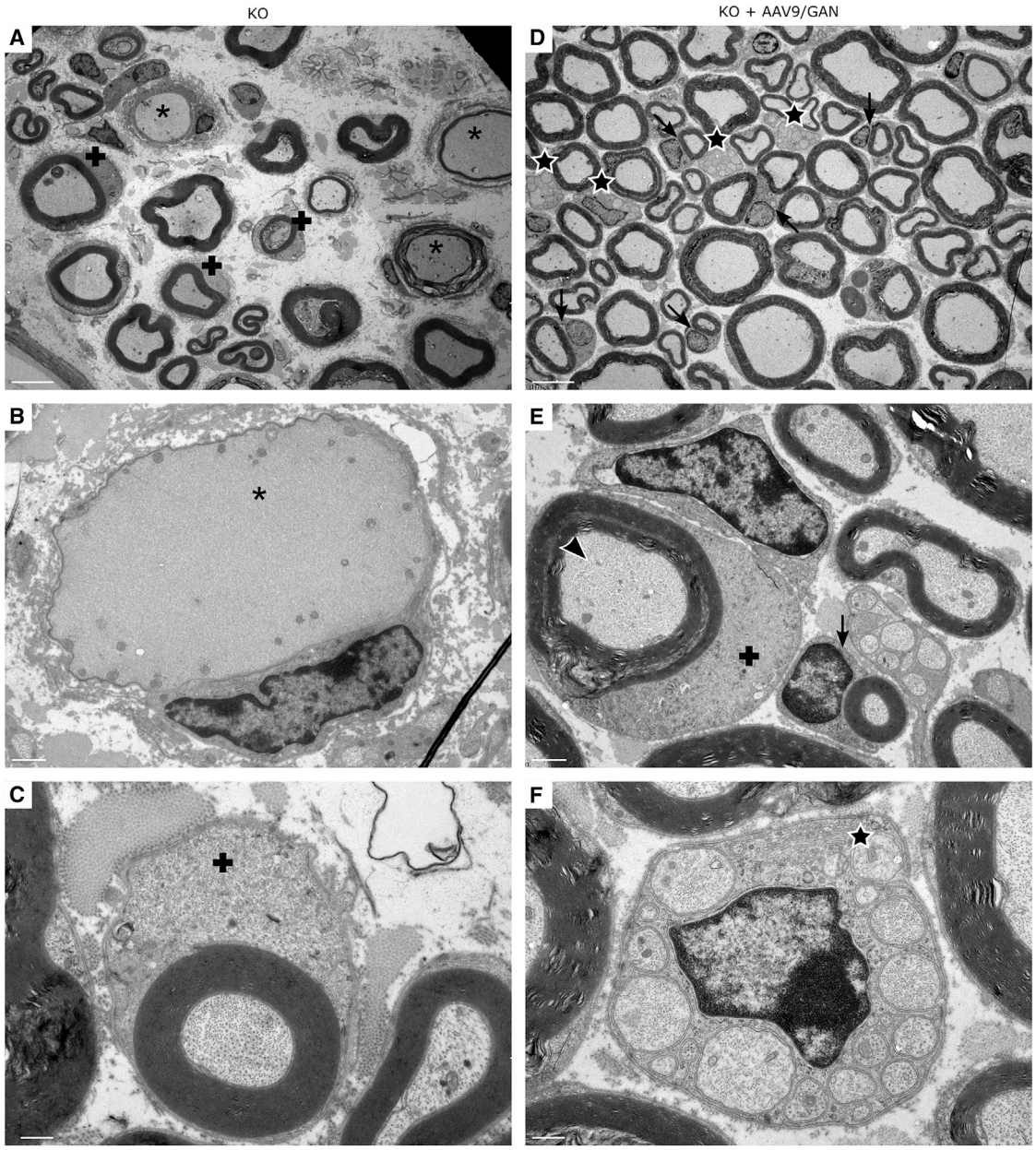

Figure 7. AAV9/JeT-GAN Gene Therapy Improves IF Cytoskeleton in GAN Peripheral Nerves

EM examination of sciatic nerves from 24-month-old control GAN/Y KO and AAV9/JeT-FLAG-GAN-injected GAN/Y KO mice at 6 months post-IT-injection (cohort 4). (A–C) Control GAN KO mouse and (D–F) *GAN*-treated GAN KO mouse. Stars indicate intact unmyelinated fibers and associated Schwann cells, arrows indicate normal Schwann cell cytoplasm associated with myelinated fibers, asterisks indicate dense, disorganized accumulations of NFs in fibers, arrowhead indicates increased density of NFs in myelinated fiber, and crosses indicate accumulation of IFs in Schwann cell cytoplasm associated with myelinated fibers. Representative images from n = 6 per group. Scale bar: 5 μm (A and D), 1 μm (B and E), and 0.5 μm (C and F).

Patient Fibroblast Assays

GAN fibroblasts were treated with AAV and assayed for IF arrangement as described.[22] Primary antibodies used were anti-vimentin (1:1,000) (Millipore, CBL202) and anti-GFP (1:500) (Millipore, 3080). Secondary antibodies were goat anti-mouse Alexa 594 (1:10,000) (Invitrogen, A11032) and goat anti-rabbit Alexa 488 (1:10,000) (Invitrogen, A11008). The presence of vimentin aggregates were scored visually, with >500 cells typically assessed per coverslip.

Mice

GAN KO breeders with a deletion of *GAN* exons 3–5 (GAN/Y) were obtained from Y. Yang,[33] and GAN KO breeders with a deletion of

GAN exon 1 (GAN/J) were obtained from J.P. Julien;[34] both lines were maintained at UNC. Heterozygous GAN mice were phenotypically normal, and age-matched littermates were used as normal controls; animals were genotyped as described previously.[33,34] Both sexes were used in these studies. See Table 1 for injection cohorts and details on final animal numbers, ages of injection, vector doses, and assays for each cohort. There is an increased incidence of ulcerative dermatitis and weight loss in aged GAN/Y mice,[33] so criteria for early euthanasia of mice in this study included greater than 20% loss of their maximum body weight or ulcerative dermatitis. For cohort 2 GAN/Y mice, an n = 10 of mice were originally enrolled per treatment group. Two of the AAV9/JeT-GAN-injected mice were euthanized prior to the start of rotarod testing, and one mouse was euthanized before 22 months of age. For the control KO group, one animal was euthanized prior to the beginning of rotarod testing, one mouse was euthanized before 20 months of age, one was euthanized before 21 months of age, and two were euthanized before 22 months of age.

Injections

Direct Brain

Intra-cranial injections were performed as described,[43] using the following stereotaxic coordinates, relative to bregma: rostral/caudal, +0.5 mm (toward rostral); left/right, left +3.5 mm; up/down, −3.5 mm. A total volume of 1 μL was delivered over 10 min.

IT

AAV9 vectors were diluted in vehicle containing 5%–10% lidocaine as a readout of the success of the injection, and 5 μL was injected in each animal. The injection was performed by lumbar puncture as described.[43]

Brain IF Assessment

Injected mouse brains were isolated and analyzed by IHC as previously described.[44] Primary antibodies were anti-NF heavy (1:1,000) (Covance, SMI-32) and anti-GFP (1:500) (Millipore, 3080). IF inclusions were quantified by taking the ratio of the inclusions in the injected hemisphere versus the inclusions in the uninjected hemisphere in areas highly transduced by AAV9 (cortex and striatum) and in a control area with low transduction.

Rotarod

Starting at 16–20 months of age, the UNC mouse behavioral phenotyping core tested mice on an accelerating rotarod (Ugo Basile, Stoelting), and testers were blind to genotype and treatment. For the first test session, mice received three training trials with at least 45 s between each trial, and for each trial, the rod accelerated from 3 rpm to 30 rpm across 5 min (the maximum trial length). Forty-eight hours after training, mice underwent a two-trial retest and then received a monthly two-trial retest until a maximum of 24 months of age. There was no difference in the performance of uninjected and vehicle-injected normal GAN/Y mice, and results were combined to increase statistical power (Figure S7). In cohort 2, one vehicle-treated KO mouse and one AAV9/JeT-GAN-treated mouse were excluded from analyses due to a refusal to perform the rotarod task.

Vector Biodistribution and Gigaxonin Expression

Mice were deeply anesthetized with an overdose of avertin (0.04 mL/g of a 1.25% solution) and perfused with PBS containing 1 μg/mL heparin. Tissues were quickly dissected, immediately frozen on dry ice, and stored at −80°C. For vector biodistribution, DNA was extracted and quantified by qPCR as previously described.[30] Data is reported as the number of double-stranded GANopt DNA molecules per two double-stranded copies of the mouse LaminB2 locus, which is the number of vector DNA copies per diploid mouse genome. For gigaxonin mRNA transcript expression, the methods used for RNA extraction, reverse transcription, and quantification by qRT-PCR have been previously described.[22] Codon-optimized gigaxonin transcript expression was normalized to that of endogenous mouse β-actin. For gigaxonin protein expression in treated mice, lumbar cord was homogenized in lysis buffer (50 mM Tris-HCl [pH 7.5], 150 mM NaCl, 100 μM DTT, 1 mM PMSF, 1% protease inhibitors cocktail [Thermo Scientific], and 1% phosphatase inhibitor cocktails 2 and 3 Sigma]) and centrifuged at 16,000 × *g* for 15 min at 4°C. The supernatants were transferred to a new tube, and the protein concentration was determined using a BCA protein assay (Pierce). For each animal, 80 μg of protein was loaded onto 10% Tris-Glycine gels (Bio-Rad), separated by SDS-PAGE, and transferred to nitrocellulose membranes. Western blotting was performed as described in the Vector Expression Studies in Cells section.

DRG Light Microscopy

Mice were perfused with PBS containing 1 U/mL heparin followed by 4% paraformaldehyde, then tissues were drop fixed in 10% formalin. Whole spines were de-calcified overnight in Formical-4, the lumbar region was paraffin embedded, and 5 μm sections were stained with H&E. Neuronal counts were performed based on the identification of nuclei and nucleoli within neuronal cell bodies,[45] with the counter blind to genotype and treatment. The ratio of the number of neurons containing IF inclusions versus the total number of neurons within the ganglia was determined as a measurement of neuronal perikaryal IF inclusions for each DRG. Images were captured at 65× with oil immersion using the Olympus BX61 microscope (Olympus America), the QImaging Retiga 4000R camera (Surrey), and Volocity 6.2.1 software (Perkin Elmer).

Sciatic Nerve EM

Mice were perfused with PBS containing 1 U/mL heparin, followed by 2% paraformaldehyde/2.5% glutaraldehyde/0.15 M sodium phosphate (pH 7.4). Proximal and distal segments of the right and left sciatic nerves were dissected, processed, and sectioned by the EM core facility at UNC as described.[46] Semi-thick sections (1 μm) were stained with toluidine blue. Ultrathin sections (70–80 nm) were mounted on formvar/carbon-coated 75 mesh copper grids and stained with 4% aqueous uranyl acetate for 12 min and lead citrate for 8 min. Digital images were obtained using a LEO EM910 transmission EM operating at 80 kV (Carl Zeiss Microscopy, Thornwood, NY) with a Gatan Orius SC1000 CCD Digital Camera and with Digital Micrograph software version 2.3.1 (Gatan, Pleasanton, CA).

Statistical Analysis

Student's unpaired t test was used to compare single means. One-way ANOVA was used to compare multiple means with Bonferonni's post-hoc analysis. Behavioral data were first analyzed using two-way ANOVA, with factors genotype or treatment and age. Significant effects of genotype, treatment, or age in the overall analyses were further investigated with Bonferonni's post-hoc analysis of each testing age. For all comparisons, statistical significance was set at $p < 0.05$. Data were analyzed and graphed using GraphPad Prism software (v. 6.04; GraphPad Software).

Study Approval

Animal studies were performed in strict accordance with the Guide for the Care and Use of Laboratory Animals of the NIH (DHHS Publication no. [NIH] 85-23). The Institutional Animal Care and Use Committee of UNC Chapel Hill approved the protocol.

SUPPLEMENTAL INFORMATION

Supplemental Information includes seven figures and one table and can be found with this article online at https://doi.org/10.1016/j.omtm.2018.02.005.

AUTHOR CONTRIBUTIONS

R.M.B., D.A., and S.J.G. contributed to study concept and design. R.M.B., D.A., S.N.K., and S.J.G. contributed to data acquisition and analysis. R.M.B, D.A., and S.J.G. contributed to drafting the text and figures.

CONFLICTS OF INTEREST

S.J.G. has received patent royalties for intellectual property (IP) licensed to Asklepios Biopharma, but this IP was not used in this study. Asklepios has licenses for other IP that was used in this study.

ACKNOWLEDGMENTS

This study was supported by Hannah's Hope Fund, the NIH National Institute of Neurological Disorders and Stroke (NS087175, S.J.G.; NS095515, R.M.B.), and the NIH National Institute of Child Health and Human Development (HD040127, R.M.B.; U54HD079124, the Mouse Behavioral Phenotyping Laboratory of the UNC IDDRC). Indirect administrative support for S.J.G. was provided by the Research to Prevent Blindness to the UNC-CH Department of Ophthalmology. The UNC-CH Translational Pathology Laboratory (TPL) and the LCCC Animal Studies Core are supported, in part, by an NCI Center Core Support Grant (CA16086) to the UNC Lineberger Comprehensive Cancer Center. We thank L. Bachaboina, J.C. Fox, and M. Keener for technical support with animal care, necropsies, histology, and early vector assessments and V. Zaric for technical support with qPCR and qRT-PCR analyses. We acknowledge K. Burns at UNC-CH, the Microscopy Services Laboratory, Department of Pathology and Laboratory Medicine at UNC-CH, and the Mouse Behavioral Phenotyping Laboratory of the UNC IDDRC. We thank B. Midkiff in the UNC-CH TPL for technical assistance. Intracranial injections were performed within the UNC-CH LCCC Animal Studies Core Facility. We thank Dr. Y. Yang (Stanford University, USA) for providing the GAN/Y mice and Dr. J.P. Julien (Universite Laval, Canada) for providing the GAN/J mice. We thank Dr. J. Samulski for insightful discussions and the use of UNC Gene Therapy Center resources/equipment, as well as the UNC-CH Vector Core facility for the production of some vectors used in these studies. Finally, we thank Dr. C. Bönnemann and his team at NIH/NINDS for their collaboration and the initiation of the phase 1 GAN clinical trial.

REFERENCES

1. Asbury, A.K., Gale, M.K., Cox, S.C., Baringer, J.R., and Berg, B.O. (1972). Giant axonal neuropathy—a unique case with segmental neurofilamentous masses. Acta Neuropathol. *20*, 237–247.
2. Berg, B.O., Rosenberg, S.H., and Asbury, A.K. (1972). Giant axonal neuropathy. Pediatrics *49*, 894–899.
3. Yang, Y., Allen, E., Ding, J., and Wang, W. (2007). Giant axonal neuropathy. Cell. Mol. Life Sci. *64*, 601–609.
4. Peiffer, J., Schlote, W., Bischoff, A., Boltshauser, E., and Müller, G. (1977). Generalized giant axonal neuropathy: a filament-forming disease of neuronal, endothelial, glial, and schwann cells in a patient without kinky hair. Acta Neuropathol. *40*, 213–218.
5. Houlden, H., Groves, M., Miedzybrodzka, Z., Roper, H., Willis, T., Winer, J., Cole, G., and Reilly, M.M. (2007). New mutations, genotype phenotype studies and manifesting carriers in giant axonal neuropathy. J. Neurol. Neurosurg. Psychiatry *78*, 1267–1270.
6. Yiu, E.M., and Ryan, M.M. (2012). Genetic axonal neuropathies and neuronopathies of pre-natal and infantile onset. J. Peripher. Nerv. Syst. *17*, 285–300.
7. Johnson-Kerner, B.L., Roth, L., Greene, J.P., Wichterle, H., and Sproule, D.M. (2014). Giant axonal neuropathy: An updated perspective on its pathology and pathogenesis. Muscle Nerve *50*, 467–476.
8. Mahammad, S., Murthy, S.N., Didonna, A., Grin, B., Israeli, E., Perrot, R., Bomont, P., Julien, J.P., Kuczmarski, E., Opal, P., and Goldman, R.D. (2013). Giant axonal neuropathy-associated gigaxonin mutations impair intermediate filament protein degradation. J. Clin. Invest. *123*, 1964–1975.
9. Igisu, H., Ohta, M., Tabira, T., Hosokawa, S., and Goto, I. (1975). Giant axonal neuropathy. A clinical entity affecting the central as well as the peripheral nervous system. Neurology *25*, 717–721.
10. Ouvrier, R.A. (1989). Giant axonal neuropathy. A review. Brain Dev. *11*, 207–214.
11. Mohri, I., Taniike, M., Yoshikawa, H., Higashiyama, M., Itami, S., and Okada, S. (1998). A case of giant axonal neuropathy showing focal aggregation and hypophosphorylation of intermediate filaments. Brain Dev. *20*, 594–597.
12. Cleveland, D.W., Yamanaka, K., and Bomont, P. (2009). Gigaxonin controls vimentin organization through a tubulin chaperone-independent pathway. Hum. Mol. Genet. *18*, 1384–1394.
13. Pena, S.D., Opas, M., Turksen, K., Kalnins, V.I., and Carpenter, S. (1983). Immunocytochemical studies of intermediate filament aggregates and their relationship to microtubules in cultured skin fibroblasts from patients with giant axonal neuropathy. Eur. J. Cell Biol. *31*, 227–234.
14. Kantor, B., Bailey, R.M., Wimberly, K., Kalburgi, S.N., and Gray, S.J. (2014). Methods for gene transfer to the central nervous system. Adv. Genet. *87*, 125–197.
15. Hocquemiller, M., Giersch, L., Audrain, M., Parker, S., and Cartier, N. (2016). Adeno-associated virus-based gene therapy for CNS diseases. Hum. Gene Ther. *27*, 478–496.
16. Murlidharan, G., Samulski, R.J., and Asokan, A. (2014). Biology of adeno-associated viral vectors in the central nervous system. Front. Mol. Neurosci. *7*, 76.
17. Federici, T., Taub, J.S., Baum, G.R., Gray, S.J., Grieger, J.C., Matthews, K.A., Handy, C.R., Passini, M.A., Samulski, R.J., and Boulis, N.M. (2012). Robust spinal motor neuron transduction following intrathecal delivery of AAV9 in pigs. Gene Ther. *19*, 852–859.
18. Samaranch, L., Salegio, E.A., San Sebastian, W., Kells, A.P., Foust, K.D., Bringas, J.R., Lamarre, C., Forsayeth, J., Kaspar, B.K., and Bankiewicz, K.S. (2012). Adeno-associated virus serotype 9 transduction in the central nervous system of nonhuman primates. Hum. Gene Ther. *23*, 382–389.

19. Gray, S.J., Nagabhushan Kalburgi, S., McCown, T.J., and Jude Samulski, R. (2013). Global CNS gene delivery and evasion of anti-AAV-neutralizing antibodies by intrathecal AAV administration in non-human primates. Gene Ther. *20*, 450–459.

20. Passini, M.A., Bu, J., Richards, A.M., Treleaven, C.M., Sullivan, J.A., O'Riordan, C.R., Scaria, A., Kells, A.P., Samaranch, L., San Sebastian, W., et al. (2014). Translational fidelity of intrathecal delivery of self-complementary AAV9-survival motor neuron 1 for spinal muscular atrophy. Hum. Gene Ther. *25*, 619–630.

21. Meyer, K., Ferraiuolo, L., Schmelzer, L., Braun, L., McGovern, V., Likhite, S., Michels, O., Govoni, A., Fitzgerald, J., Morales, P., et al. (2015). Improving single injection CSF delivery of AAV9-mediated gene therapy for SMA: a dose-response study in mice and nonhuman primates. Mol. Ther. *23*, 477–487.

22. Mussche, S., Devreese, B., Nagabhushan Kalburgi, S., Bachaboina, L., Fox, J.C., Shih, H.J., Van Coster, R., Samulski, R.J., and Gray, S.J. (2013). Restoration of cytoskeleton homeostasis after gigaxonin gene transfer for giant axonal neuropathy. Hum. Gene Ther. *24*, 209–219.

23. Johnson-Kerner, B.L., Ahmad, F.S., Diaz, A.G., Greene, J.P., Gray, S.J., Samulski, R.J., Chung, W.K., Van Coster, R., Maertens, P., Noggle, S.A., et al. (2015). Intermediate filament protein accumulation in motor neurons derived from giant axonal neuropathy iPSCs rescued by restoration of gigaxonin. Hum. Mol. Genet. *24*, 1420–1431.

24. Israeli, E., Dryanovski, D.I., Schumacker, P.T., Chandel, N.S., Singer, J.D., Julien, J.P., Goldman, R.D., and Opal, P. (2016). Intermediate filament aggregates cause mitochondrial dysmotility and increase energy demands in giant axonal neuropathy. Hum. Mol. Genet. *25*, 2143–2157.

25. Tornøe, J., Kusk, P., Johansen, T.E., and Jensen, P.R. (2002). Generation of a synthetic mammalian promoter library by modification of sequences spacing transcription factor binding sites. Gene *297*, 21–32.

26. Levitt, N., Briggs, D., Gil, A., and Proudfoot, N.J. (1989). Definition of an efficient synthetic poly(A) site. Genes Dev. *3*, 1019–1025.

27. McCarty, D.M., Monahan, P.E., and Samulski, R.J. (2001). Self-complementary recombinant adeno-associated virus (scAAV) vectors promote efficient transduction independently of DNA synthesis. Gene Ther. *8*, 1248–1254.

28. McCarty, D.M., Fu, H., Monahan, P.E., Toulson, C.E., Naik, P., and Samulski, R.J. (2003). Adeno-associated virus terminal repeat (TR) mutant generates self-complementary vectors to overcome the rate-limiting step to transduction in vivo. Gene Ther. *10*, 2112–2118.

29. McCarty, D.M. (2008). Self-complementary AAV vectors; advances and applications. Mol. Ther. *16*, 1648–1656.

30. Gray, S.J., Matagne, V., Bachaboina, L., Yadav, S., Ojeda, S.R., and Samulski, R.J. (2011). Preclinical differences of intravascular AAV9 delivery to neurons and glia: a comparative study of adult mice and nonhuman primates. Mol. Ther. *19*, 1058–1069.

31. Pena, S.D. (1981). Giant axonal neuropathy: intermediate filament aggregates in cultured skin fibroblasts. Neurology *31*, 1470–1473.

32. Bomont, P. (2016). Degradation of the intermediate filament family by gigaxonin. Methods Enzymol. *569*, 215–231.

33. Ding, J., Allen, E., Wang, W., Valle, A., Wu, C., Nardine, T., Cui, B., Yi, J., Taylor, A., Jeon, N.L., et al. (2006). Gene targeting of GAN in mouse causes a toxic accumulation of microtubule-associated protein 8 and impaired retrograde axonal transport. Hum. Mol. Genet. *15*, 1451–1463.

34. Dequen, F., Bomont, P., Gowing, G., Cleveland, D.W., and Julien, J.P. (2008). Modest loss of peripheral axons, muscle atrophy and formation of brain inclusions in mice with targeted deletion of gigaxonin exon 1. J. Neurochem. *107*, 253–264.

35. Ganay, T., Boizot, A., Burrer, R., Chauvin, J.P., and Bomont, P. (2011). Sensory-motor deficits and neurofilament disorganization in gigaxonin-null mice. Mol. Neurodegener. *6*, 25.

36. Hadaczek, P., Eberling, J.L., Pivirotto, P., Bringas, J., Forsayeth, J., and Bankiewicz, K.S. (2010). Eight years of clinical improvement in MPTP-lesioned primates after gene therapy with AAV2-hAADC. Mol. Ther. *18*, 1458–1461.

37. Samaranch, L., Salegio, E.A., San Sebastian, W., Kells, A.P., Bringas, J.R., Forsayeth, J., and Bankiewicz, K.S. (2013). Strong cortical and spinal cord transduction after AAV7 and AAV9 delivery into the cerebrospinal fluid of nonhuman primates. Hum. Gene Ther. *24*, 526–532.

38. Sorrentino, N.C., Maffia, V., Strollo, S., Cacace, V., Romagnoli, N., Manfredi, A., Ventrella, D., Dondi, F., Barone, F., Giunti, M., et al. (2016). A comprehensive map of CNS transduction by eight recombinant adeno-associated virus serotypes upon cerebrospinal fluid administration in pigs. Mol. Ther. *24*, 276–286.

39. King, R.H.M. (2006). The pathology of peripheral nerve diseases. Adv. Clin. Neurosci. Rehabil. *6*, 16–18.

40. Tandan, R., Little, B.W., Emery, E.S., Good, P.S., Pendlebury, W.W., and Bradley, W.G. (1987). Childhood giant axonal neuropathy. Case report and review of the literature. J. Neurol. Sci. *82*, 205–228.

41. Midroni, G., and Bilbao, J.M. (1995). Biopsy Diagnosis of Peripheral Neuropathy (Butterworth-Heinmann), pp. 45–74.

42. Clément, N., and Grieger, J.C. (2016). Manufacturing of recombinant adeno-associated viral vectors for clinical trials. Mol. Ther. Methods Clin. Dev. *3*, 16002.

43. Gray, S.J., Choi, V.W., Asokan, A., Haberman, R.A., McCown, T.J., and Samulski, R.J. (2011). Production of recombinant adeno-associated viral vectors and use in in vitro and in vivo administration. Curr. Protoc. Neurosci. *4*, 4.17.

44. Karumuthil-Melethil, S., Nagabhushan Kalburgi, S., Thompson, P., Tropak, M., Kaytor, M.D., Keimel, J.G., Mark, B.L., Mahuran, D., Walia, J.S., and Gray, S.J. (2016). Novel vector design and hexosaminidase variant enabling self-complementary adeno-associated virus for the treatment of Tay-Sachs disease. Hum. Gene Ther. *27*, 509–521.

45. Lawson, S.N. (1979). The postnatal development of large light and small dark neurons in mouse dorsal root ganglia: a statistical analysis of cell numbers and size. J. Neurocytol. *8*, 275–294.

46. Karumuthil-Melethil, S., Marshall, M.S., Heindel, C., Jakubauskas, B., Bongarzone, E.R., and Gray, S.J. (2016). Intrathecal administration of AAV/GALC vectors in 10-11-day-old twitcher mice improves survival and is enhanced by bone marrow transplant. J. Neurosci. Res. *94*, 1138–1151.

OMTM, Volume *9*

Supplemental Information

Development of Intrathecal AAV9 Gene Therapy for Giant Axonal Neuropathy

Rachel M. Bailey, Diane Armao, Sahana Nagabhushan Kalburgi, and Steven J. Gray

Supplementary Material:

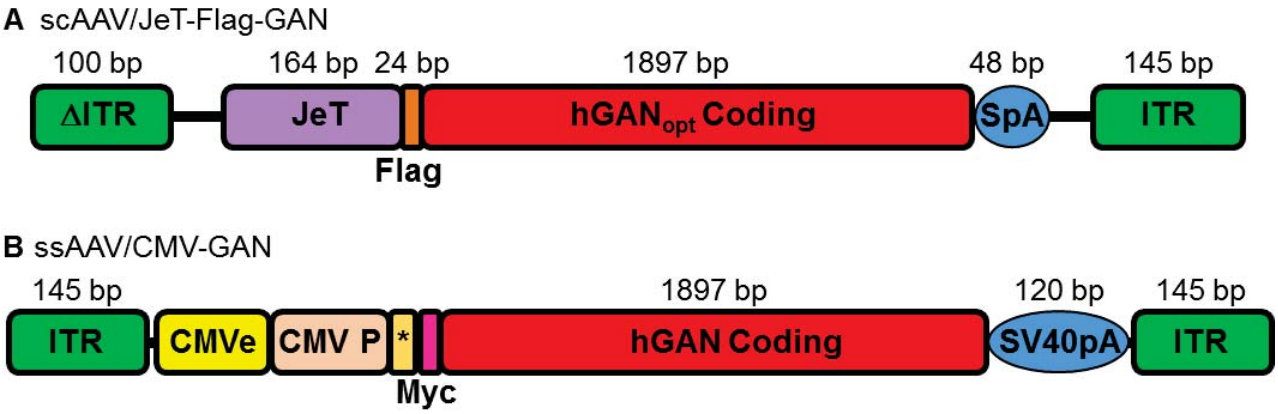

Figure S1. Design of additional vectors used in studies. (A) Schematic diagram of the self-complementary (sc) AAV/JeT-Flag-GAN gene transfer cassette using a JeT promoter, an n-terminal flag tag on full length, codon-optimized human GAN cDNA and the synthetic polyA tail (SpA). (B) Schematic diagram of the single-stranded (ss) AAV/CMV-GAN gene transfer cassette using a CMV enhancer (CMVe) and promoter (CMV P), chimeric intron (*), an N-terminal myc tag on full length, WT human GAN cDNA and the SV40 polyA tail (SV40pA).

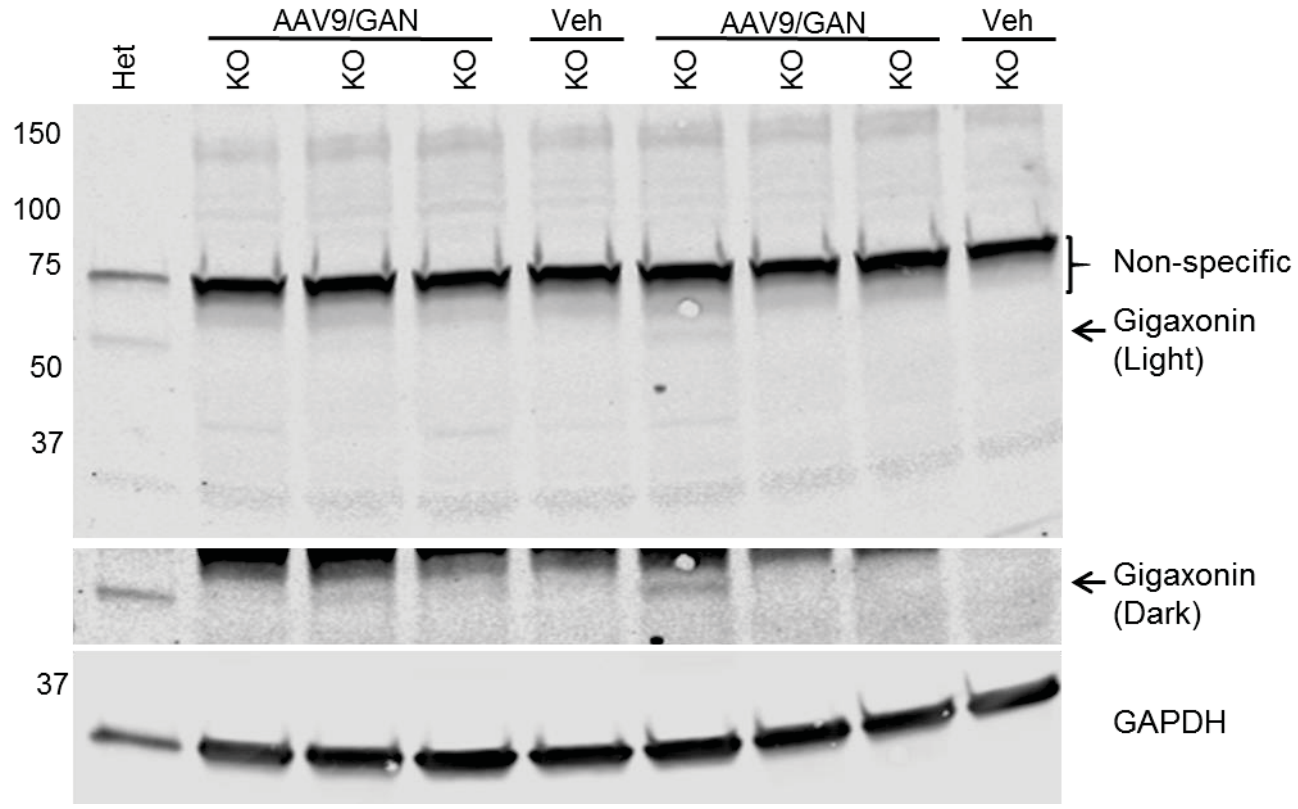

Figure S2. Gigaxonin expression in the lumbar cord of AAV9/JeT-GAN treated GAN/J KO mice. Gigaxonin protein is detected in the lumbar cord of GAN/J KO mice ~ 10 months after a single IT injection of AAV9/JeT-GAN and absent in vehicle injected littermates (cohort 3). Western blots of gigaxonin and GAPDH in heterozygous (het), and either vehicle (Veh) or AAV9/GAN injected KO mice. Top panel = light exposure of gigaxonin expression; middle panel = dark exposure of gigaxonin expression; and bottom panel = GAPDH expression.

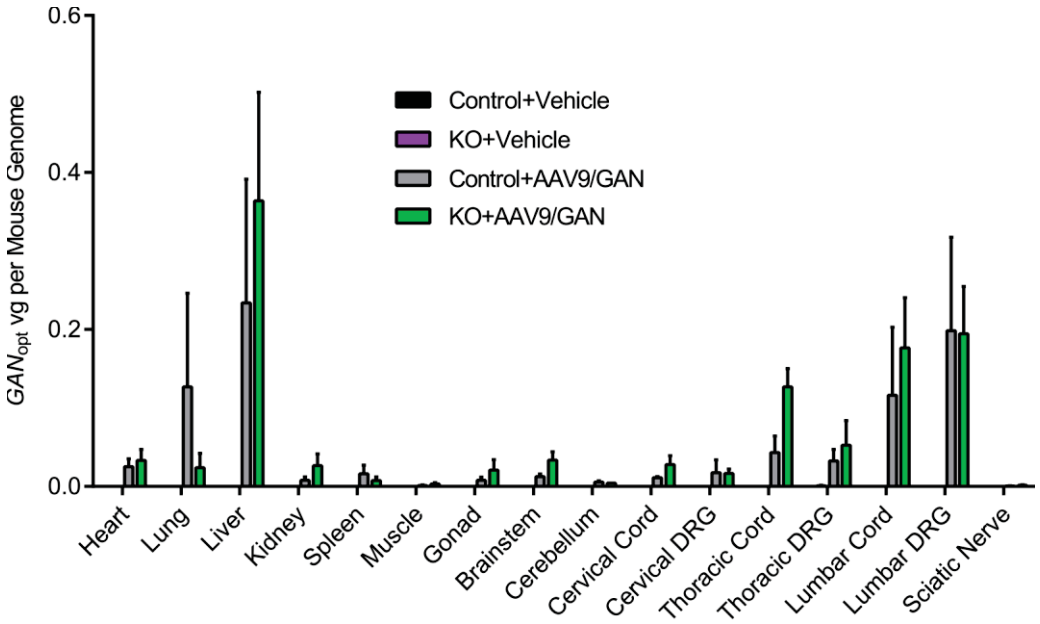

Figure S3. AAV9/JeT-GAN biodistribution in IT injected GAN/J control and KO mice. Vector biodistribution of AAV9/JeT-GAN in GAN/J mice injected at 14-16-months-of-age and harvested at 24-months-of-age (cohort 3) was assessed by measuring the codon-optimized human GAN (GAN_{opt}) vector DNA in each tissue sample. Mouse LaminB2 was measured as an internal control and was detected in all samples. Data are means ± SEM for each group (GAN/J: $n = 3$ per group).

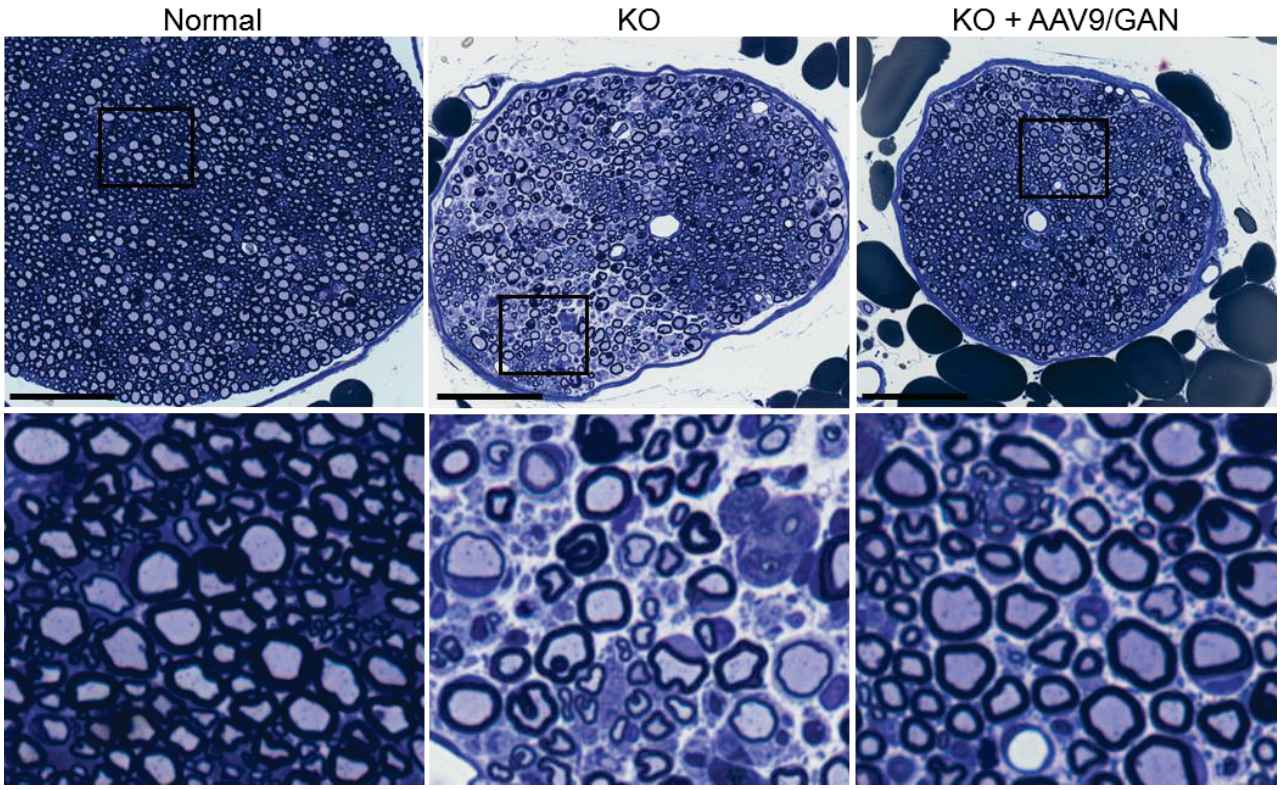

Figure S4. GAN gene therapy improves GAN sciatic nerve pathology. Representative images of 1 μm thick toluidine blue-stained sciatic nerve sections from 24-month-old normal control mice (left), control GAN/Y KO mice (middle) or GAN/Y KO mice injected with AAV9/JeT-Flag-GAN (right) at 18 months of age (cohort 4). Representative images from $n = 3$ per normal control group and 6 per each GAN group. Boxes indicate area magnified in corresponding frame below. Scale bars represent 70 μm.

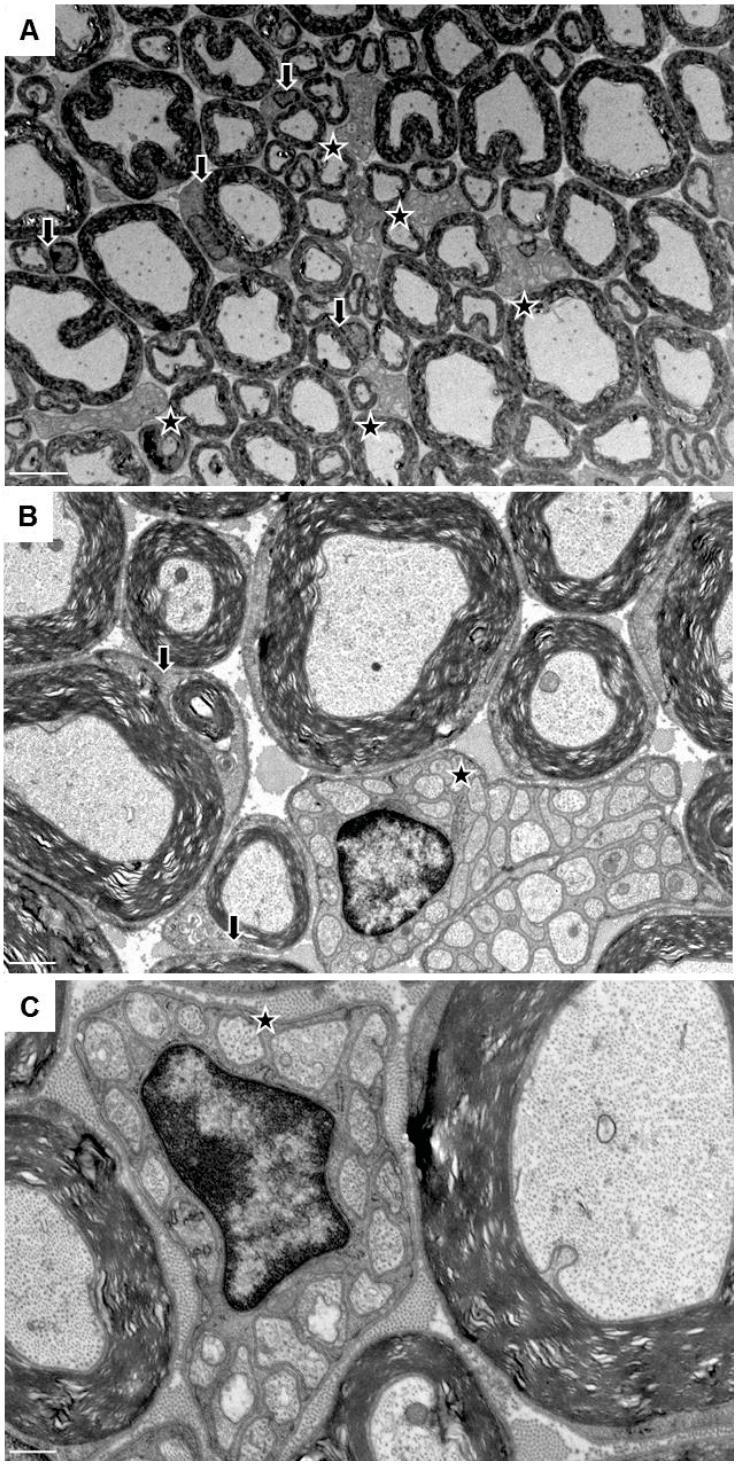

Figure S5. Normal sciatic nerves from control mice. EM examination of sciatic nerves from 24-month-old normal control mice (cohort 4). Stars indicate intact unmyelinated fibers and associated Schwann cells and arrows indicate normal Schwann cell cytoplasm associated with myelinated fibers. Representative images from $n = 3$ mice. Scale bar: 5 μm (A), 1 μm (B) and 0.5 μm (C).

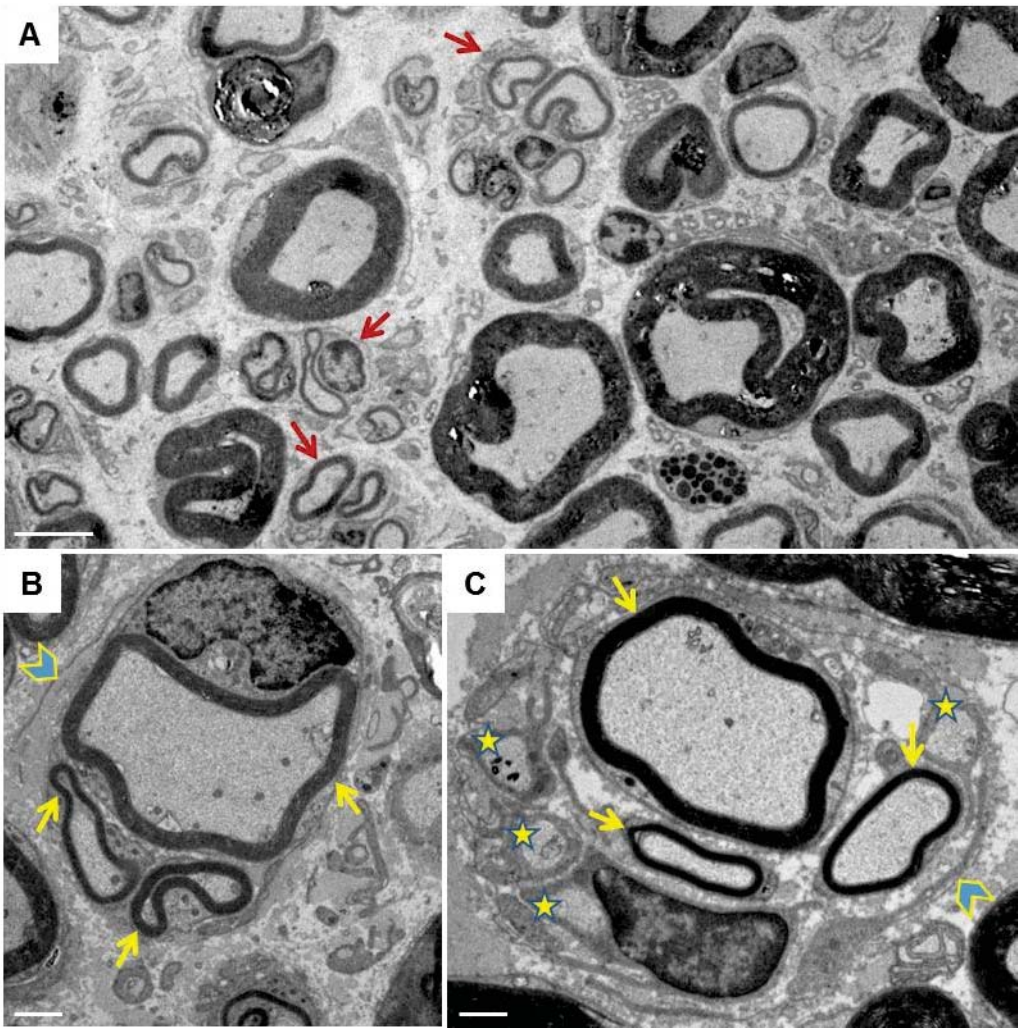

Figure S6. AAV9/JeT-GAN gene therapy reveals axonal regeneration in GAN nerves. EM examination of sciatic nerves from AAV9/JeT-GAN injected GAN/Y KO mice at 6 months post IT injection (cohort 4) (A-C). (A) Arrows indicate regenerating clusters. (B, C) Arrows indicate closely apposed conFigureurations of regenerating myelinated fibers, stars indicate regenerating unmyelinated fibers and arrowheads indicate discontinuous basal lamina belonging to the original degenerated fiber and surrounding the regenerating clusters. Representative images from $n = 6$. Scale bars: 5 µm (A), 1 µm (B, C).

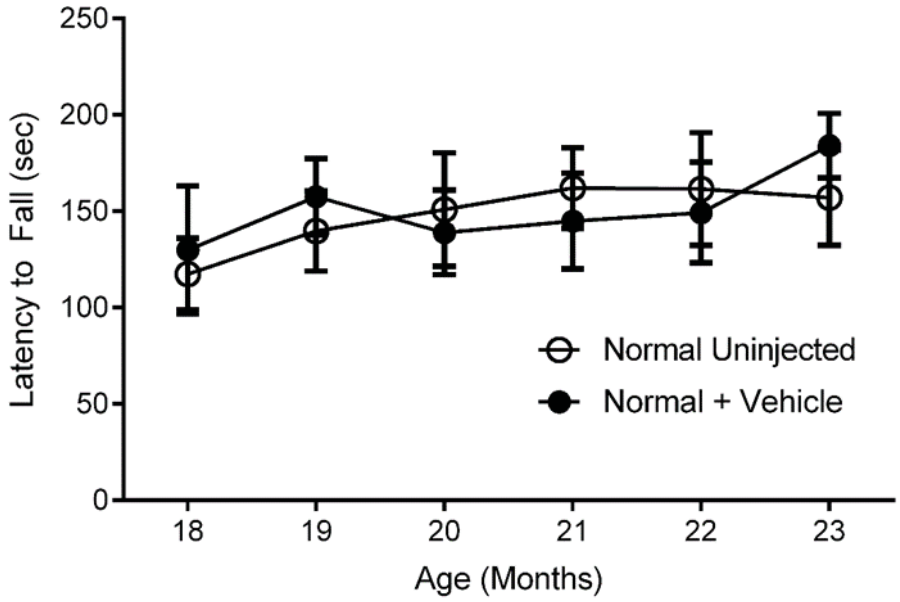

Figure S7. Intrathecal injection does not affect rotarod performance. Using the accelerating rotarod, no difference in rotarod performance was found in aged uninjected mice and mice that received a vehicle IT injection (cohort 2). Data shown are means ± SEM for each group (n = 8-10).

Table S1. Use of GAN viral vectors discussed in text.

Vector	In vitro Application	In vivo Application
scAAV/JeT-GAN	Expression studies and IF clearance in patient fibroblasts	IT injection studies in GAN KO mice for pathological and functional treatment studies
scAAV/JeT-Flag-GAN	Expression studies and IF clearance in patient fibroblasts	IT injection in GAN KO mice for sciatic nerve rescue and direct brain injection studies to assess NF clearance.
ssAAV/CMV-GAN	IF clearance in patient fibroblasts	